On the ability of statistical wind-wave models to capture the variability and long-term trends of the North Atlantic winter wave climate

Adrián Martínez-Asensio*[1], Marta Marcos[1], Michael N. Tsimplis[2], Gabriel Jordà[1,2], Xiangbo Feng[3], Damià Gomis[1]

[1] IMEDEA(UIB-CSIC), Spain
[2] National Oceanography Center, Southampton, UK
[3] Department of Meteorology, University of Reading, UK.

*Corresponding author: adrian.martinez@uib.es

Abstract

A dynamical wind-wave climate simulation covering the North Atlantic Ocean and spanning the whole 21st century under the A1B scenario has been compared with a set of statistical projections using atmospheric variables or large scale climate indices as predictors. As a first step, the performance of all statistical models has been evaluated for the present-day climate; namely they have been compared with a dynamical wind-wave hindcast in terms of winter Significant Wave Height (SWH) trends and variance as well as with altimetry data. For the projections, it has been found that statistical models that use wind speed as independent variable predictor are able to capture a larger fraction of the winter SWH inter-annual variability (68% on average) and of the long term changes projected by the dynamical simulation. Conversely, regression models using climate indices, sea level pressure and/or pressure gradient as predictors, account for a smaller SWH variance (from 2.8% to 33%) and do not reproduce the dynamically projected long term trends over the North Atlantic. Investigating the wind-sea and swell components separately, we have found that the combination of two regression models, one for wind-sea waves and another one for the swell component, can improve significantly the wave field projections obtained from single regression models over the North Atlantic.

1. Introduction

Changes in wave climate have received much attention in recent years due to their impact on coastal and offshore structures and ecosystems. Numerous wave climate simulations under different future scenarios of greenhouse gases (GHGs) emissions have been generated at both global and regional scales using numerical wave models. The North Atlantic is one of the most widely studied regions. Many earlier works have pointed to changes in wave height climate as a consequence of global warming. For example, Mori et al. (2010) projected future decreases in the wave heights over the North Atlantic at mid-latitudes by using wind fields generated by the MRI-JMA General Circulation Model (GCM) run under the A1B scenario. Likewise, Hemer et al. (2012) projected future decreases in wave heights during winter and changes in wave directions over all the North Atlantic by using the ECHAM5 GCM and CSIRO Mk3.5 GCM wind fields, both under the A2 forcing scenario. Semedo et al. (2013) projected decreases in both wave heights and periods over the North Atlantic during the winter season by using ECHAM5 GCM wind fields under the A1B scenario. Fan et al. (2013) projected decreases of wave heights during winter over the North Atlantic and increases over the north-eastern sector by using a three member ensemble forced by CM2 GCM, HadCM3 GCM and ECHAM5 GCM wind fields under the A1B scenario. In a subsequent paper, Fan et al. (2014) used the same model ensemble to obtain winter trends for the wind-sea and swell components separately. Andrade et al. (2007) projected decreases of wave heights and clockwise changes in wave directions and investigated their effects along the Portuguese coast. More local studies also exist in the region. In particular, Charles et al. (2012) projected very similar winter wave height decreases over the Bay of Biscay by using the ARPEGE-Climat GCM under three different future climate scenarios (B1, A1B, A2). All the simulations referred above are based on dynamical models forced with the surface wind fields from atmospheric models. The simulated wave parameters defining the wave climate are significant wave height (SWH), mean wave period (MWP) and mean wave direction (MWD), as well as their separation into local (wind sea) and remotely-forced (swell) waves. Both components can be properly modelled when using global wind-wave models. Regional models can also be suitable to model the swell component, although they require to be nested into larger domains to account for remotely generated swell; in turn, they usually provide higher spatial resolution.

Alternative approaches to explore wave changes in future climates cover a wide variety of statistical methods that can be classified into three main types (Wilby et al., 2004): i) regression methods, ii) weather generators and iii) weather typing schemes. Each method has its own advantages and shortcomings. Briefly, weather generators are stochastic models that replicate the statistical properties of the observed sequences of events, such as mean value and variance (Ailliot et al., 2014; Wilks, 1998). Weather typing schemes establish the relationship between atmospheric and wave parameters based on a division in weather classes, as shown for instance in Camus et al., (2014). Among these, the analogue method (Lorenz, 1969; Zorita et al., 1995) and the Monte Carlo method are also weather typing methods.

Among the regression methods, the redundancy analysis used by Wang et al., (2004) to simulate future SWH changes is a first example. Some of the most frequently used regression methods are based on transfer functions, which represent the relationship between observed wave parameters, usually SWH, and atmospheric variables such as the squared wind speed ($W=u^2+v^2$), sea level pressure (P) and/or the squared sea level pressure gradient (G) representing the geostrophic wind (that is the sum of the squared zonal and squared meridional SLP gradients). The atmospheric parameters obtained from model output under increased GHG scenarios can then be used to estimate the changes in the wave field through the statistical relationship between them obtained for the present-day period, assuming that such relationship holds also for the future period. Examples of application of such methodology can be found in Wang and Swail (2006), who used global anomalies of P and G as predictors in different regression models to simulate future SWH. Likewise, Wang et al. (2010) compared both dynamical and regression models to simulate future SWH changes over the North Atlantic at hourly (dynamical) and seasonal (statistical) scales. They tested the inclusion of W as a predictor in a set of regression models, but they concluded that it was preferable to use P and G predictors to simulate future changes on SWH due to the bias in the winds produced by the atmospheric models. Wang et al., (2012) and Wang et al., (2014) improved the regression model predictability by establishing a predictor-predictand relationship at 6-hourly time scale and including the lagged-dependent variable and the Principal Components (PCs) of P and G at 6-hourly time scale as predictors, which result in a better representation of the swell. More recently, Casas-Prat et al. (2014) have developed a more complex regression model that better accounts for the swell component to simulate future changes in the wave climate of the Western Mediterranean. In a similar way to atmospheric variables, large scale climate indices can also in principle be used as proxies for the statistical projections of waves (Woolf et al., 2002; Tsimplis et al., 2005; Feng et al., 2014a). The obvious constraint is that they must be correlated for present-day climate with both wind sea and swell wave parameters (Shimura et al., 2013; Martínez-Asensio et al., in press).

The statistical techniques offer low computational effort relative to dynamical modelling, which in turn permits the generation of larger ensembles resulting in a better understanding and quantification of uncertainties. Wang and Swail (2006) carried out an analysis of the uncertainty in SWH projections over the North Atlantic by running a set of statistical simulations forced with atmospheric variables simulated by three different climate models (CGCM2, HadCM3 and ECHAM4/OPYC3) and three different scenarios (IS92a, A2 and B2) at a seasonal scale. They found that the uncertainty associated with the GCM used to feed the statistical model was much larger than that associated with the emission scenarios covering the period 1990-2049. Recently, Wang et al. (2015) reached the same conclusion by analyzing larger ensembles of statistical projections of 6-hourly SWH using Coupled Model Intercomparison Project Phase 5 (CMIP5) simulations of 6-hourly SLP. Similar conclusions were pointed out by Charles et al. (2012) by comparing their results with those available in the literature. Hemer at al. (2013) went further into the uncertainty analysis by taking into account five independent studies projecting future changes in wave climate (namely those carried out by Wang and Swail, 2006; Mori et al., 2010; Hemer et al., 2012; Semedo et al., 2013; and Fan et al., 2013). They considered a total of four climate scenarios (A2, A1B, B2 and IS92a), six GCMs (ECHAM5, CSIRO-Mk3.5, GFDL-CM2.1, HadCM3, ECHAM4 and CGCM2), an ensemble mean of three CGCM2 simulations produced with different initial conditions, two ensemble means of 18 and 23 CMIP3 members, a set of three dynamical wave models (WaveWatch III, SWAN and WAM), one statistical model and three wave parameters (SWH, MWP and MWD). They found that the method used to obtain regional wave climates (the regional climate model, the downscaling technique, the dynamical wave model approach and the use of different predictors in statistical models) is also a high source of uncertainty.

In our study the performance of a set of transfer function statistical models to project the future wave climate over the North Atlantic Ocean is studied. Our aim is to compare a wide set of these statistical models against a reference dynamical model and quantify their performances. The chosen statistical models are based on some of the most widely used transfer functions; the set was complemented by other, more specific models as well as by models based on large scale climate indices.

A wind-wave hindcast and an atmospheric reanalysis are used to calibrate all the statistical models for the period 1958-2002. Altimetry SWH observations are used to validate both the dynamical and statistical models. Then, the atmospheric output of a climate model (ECHAM5) run under the A1B emission scenario for the period 2000-2100 is used to obtain the changes in the atmospheric parameters used as predictors in statistical models and hence for the prediction of the winter SWH fields of the future. ECHAM5 is considered one of the best CMIP3 GCMs in simulating the recent past climate conditions in terms of inter-annual variability over the North-East Atlantic (Pérez et al., 2014).

The 6-hourly surface winds output from the ECHAM5 climate model is used to force a dynamical regional wave model to project winter SWH, MWP and MWD fields. The differences between the dynamical and statistical approximations of the future wave field as well as their respective limitations are discussed.

The paper is organized as follows: the dynamical and statistical models and their forcing are presented in section 2. The models are validated for present-day climate in section 3. Projections of wave climate are presented in section 4. In the last section results are discussed and conclusions are outlined.

2. Data set and methodology

The set of dynamical and statistical simulations and the procedure to generate all of them is schematically shown in Fig. 1, while the details are given in the sections below.

2.1 Dynamical simulations

Two wind-wave hindcasts over the North Atlantic (hereinafter HE40 and HEI) were obtained by forcing a third generation wave model that explicitly solves the wave transport equation (the WAM model, see WAMDI, 1988; Günther et al., 1992) with 6-hourly surface wind fields from the atmospheric reanalysis ERA-40 (1958-2002) with a spatial resolution of 2.5x2.5 degrees and ERA-INTERIM (1989-2009) with a spatial resolution of 0.5x0.5 degrees, respectively. HE40 was used for the calibration of the statistical models, whereas HEI was used as a basis for validation purposes (more details are given in section 3). In a third simulation the WAM model was forced with 6-hourly surface wind fields (1.875x1.875 degrees of spatial resolution) from the Max Plank Institute (MPI) ECHAM5 atmospheric GCM (Roeckner et al., 2003) run for the period 1950-2100. The period 1950-2000 is a historical run forced with observed GHG concentrations (the corresponding wave simulation will be referred to as DynHist), while the period 2001-2100 is a projection under the A1B emission scenario (the corresponding wave simulation will be referred to as DynProj).

The domain of the WAM model was set to cover the North Atlantic region (from 1ºN to 67ºN and from 59ºW to 8ºE) with spatial resolution varying between 2.5 km and 50 km (see Fig. S1 in Supplementary information). Wind fields were bi-linearly interpolated onto the described model grid. This is the configuration routinely used by the Spanish Port Authority for operational purposes. The temporal resolution of the output is 3 hours. The separation of the wind-sea and swell components of the wave field is performed as in Hasselmann et al. (1996): the peaks (local maxima) of the directional wave spectrum are identified and attributed either to the sea or to the swell component depending on the period and direction of each peak. When the peak is in the same direction of the wind stress and the period is lower than 10 s, the waves are considered to be part of the wind-sea component; otherwise they are identified as swell. For the present study, all 3-hourly fields of wave parameters (SWH and its wind and swell components) corresponding to the two hindcasts HE40 and HEI and to the ECHAM simulation, were monthly averaged and bi-linearly interpolated onto a regular grid of 1x1 degree over the North Atlantic domain. At each grid point, the mean seasonal cycle of each wave parameter was obtained by averaging each calendar month during the reference period 1961-1981 and removed from all the simulations. More specifically, both HE40 and HEI anomalies were obtained by removing the mean seasonal cycle of HE40 during the reference period and DynProj anomalies were obtained by removing the mean seasonal cycle of DynHist during the same period. The resulting anomalies were used for all purposes.

2.2. Statistical simulations on a seasonal time scale

Winter (DJFM) anomaly fields (i.e., the temporal anomalies with respect to the averaged calendar month during the period 1961-1981 at each grid point defined above) of SWH from the HE40 run and of atmospheric variables from the ERA-40 reanalysis were used to estimate the regression parameters of the statistical models. Prior to the regression, 6-hourly W and P fields from ERA40 reanalysis were interpolated onto the same 1x1 grid as HE40. Subsequently, P fields were used to obtain 6-hourly G fields, i.e., as the squared sum of the zonal and meridional SLP gradients (equation 4 in the Appendix of Wang et al, 2008). These were then used to derive the seasonal quantities used in the regression model fitting.

The fact that the predictor-predictand relationships were established at the seasonal time scale while the dynamical modelling described in Section 2.1 simulates waves at a 6-hourly time scale (even if they are seasonally averaged later on) must be taken into account when quantifying the fraction of the dynamical simulation variance accounted for by the statistical models. Wang et al. (2010) compared two statistical wind-wave simulations (one forced with 12-hours wind fields and another with winter averaged fields) against seasonal wave fields of ERA-40 and found that the simulation based on seasonal relationships reproduced less variance than the simulation based on higher temporal resolution. However, this only affects the absolute values of variance accounted for, not the comparison between the different statistical models tested here, as all them are based on seasonal quantities. It is also important to note that Wang et al. (2010) did not found any difference between the two simulations in terms of winter SWH changes projected for the end of the 21st century.

The regressions followed the most commonly used models in the literature and were completed with additional models. Recently developed statistical models appropriate for higher temporal resolution fields (6-hourly or daily) have not been considered here (e.g. those developed by Wang et al., 2012 and 2014 or Casas-Prat, 2014 or Camus et al., 2014) as far as we focus on seasonal to interannual time scales. The models are listed in the following with the corresponding reference and an identification code that will be used throughout the paper:

M1: SWH = a + b*P (Wang et al., 2004)

M2: SWH = a + b*G (Wang et al., 2004)

M3: SWH = a + b*W (Wang et al., 2010)

M4: SWH = a + b*P + c*G (Wang and Swail, 2006)

M5: SWH = a + $\sum_{i=1}^{n} b_i \, PC_i \, (P)$

M6: SWH = a + $\sum_{i=1}^{n} b_i \, PC_i \, (G)$

M7: SWH = a + $\sum_{i=1}^{n} b_i \, PC_i \, (W)$

M8: SWH = a + b*P+ $\sum_{i=1}^{n} c_i \, PC_i \, (P)$

M9: SWH = a + b*G+ $\sum_{i=1}^{n} c_i \, PC_i \, (G)$ M10: SWH = a + b*W+ $\sum_{i=1}^{n} c_i \, PC_i \, (W)$

M11: SWH = a + b*P + c*G + $\sum_{i=1}^{n} d_i \, PC_i \, (P)$ + $\sum_{i=1}^{n} e_i \, PC_i \, (G)$

M12: SWH = a + b*NAO (Woolf et al., 2002)

M13: SWH = a + b*EA

M14: SWH = a + b*NAO + c*EA + d*EA/WR + e*SCAN

M15: SWHw = a + b*W

M16: SWHs = a + $\sum_{i=1}^{n} b_i \, PC_i \, (W)$

M17: SWH $= \sqrt{(< SWHw^2 > + < SWHs^2 >)}$

where *PC* in M5-M11 and M16 stands for the Principal Components obtained from a singular value decomposition of a covariance matrix (see e.g. Wallace, et al., 1992) and *n* is the number of PCs included in the model, sorted by decreasing explained variance. The P, W and G covariance matrices were computed from winter anomalies of ERA40 fields spanning the period 1958-2002 and covering the whole wave model domain. It is important to note here that the model domain includes the main areas where swells are generated, with the exception of the swells coming from the Southern Hemisphere, which can be neglected for this study. Principal Components were already used as large-scale predictors by Wang et al. (2012; 2014), in an attempt to account for changes in the swell component related to remote atmospheric forcing. Namely, Wang et al (2012) used 6-hourly time series and found that the inclusion of higher order PCs (i.e., more than 30 leading PCs) in the pool of potential predictors has trivial effects on the resulting trend estimates, though it can result in a better representation of the large-scale patterns that generate swell. Our model M11 is somewhat similar to the model of Wang et al. (2012) in the sense that both models use the PCs of P and G; however, the two models are not really comparable, because M11 is fitted to seasonal mean series instead of to 6-hourly series and moreover it does not include the lagged-dependent variable or M-order autoregressive term or the Box-Cox transformation. We chose this simplified version of the model because we deal with seasonal data, in contrast with the 6-hourly temporal resolution used by Wang et al (2012), and we do not expect significant time-lag correlations between seasons.

For each model with at least two predictors, a forward/backward stepwise regression was applied at each grid point in order to determine the number of predictors to be included (Draper and Smith, 1998) and their corresponding coefficients (see Appendix B). This procedure selects the most correlated independent variable and removes its influence through a regression analysis. Then it checks for correlation between the rest of the independent parameters and the residual signal, until the correlation becomes non-significant. When more than one predictor account for the same part of variability the regression model favours the predictor that accounts for the highest percentage of total variability. In other words, the statistical fit calculates the value of the coefficients and defines the number of parameters that optimise the fit to SWH data at each point. This also applies to the models using PCs as predictors. We have established a maximum number of PCs n=6 because for larger values the increase in explained variance was negligible (the fact that a small number of PCs is requested is due to working with seasonal values). The linear trends from all dependent and independent variables were removed before the estimation of the regression parameters.

The regression coefficients estimated for the historical period were then used to project winter SWH along the 21st century using the projected atmospheric fields of the ECHAM5 GCM. Winter (DJFM) anomaly fields of P, G and W from ECHAM5 and their corresponding PCs were used as predictors to obtain projections of winter SWH for the period 1950-2100. It is worth noting that the projected atmospheric fields are not detrended and therefore the underlying assumption is that the correlation at inter-annual scales, which determines the regression parameters, remains unaltered at lower frequencies. This means that a long term trend in the predictor will result in a trend in winter SWH with the sign and intensity given by the regression. The PCs in M5-M11 were obtained using a fixed-pattern projection approach, which consists of projecting winter anomaly fields from ECHAM5 onto the EOFs obtained from the ERA-40 reanalysis used for the regression (Wang et al., 2004). In this way, the correspondence of the regression coefficients between these so called pseudo-PCs and the original PCs used to train the model is ensured. An eventual disadvantage of the fixed-pattern projection approach is that the percentage of hindcast variability explained by each original PC is not necessarily the same than for the corresponding pseudo-PC. To check this point, we have compared the percentage of winter SWH variance accounted for in HE40 and in DynHist by the 6 leading PCs and pseudo-PCs, respectively. For the HE40 PCs we obtained variance fractions of 50% (M5 model), 41% (M6) and 68 % (M7); for the DynHist pseudo-PCs the fractions were 36%, 33% and 45%, respectively.

The climate indices considered in this work correspond to the most relevant modes of atmospheric variability over the North Atlantic, namely the North Atlantic Oscillation (NAO), East Atlantic Pattern (EA), East Atlantic/Western Russian Pattern (EA/WR) and Scandinavian Pattern (SCAN). The climate indices were obtained for the same period than the atmospheric parameters (1958-2002) using P fields from ERA-40. Monthly anomalies of P fields over the Northern Hemisphere (20ºN-90ºN) were first computed removing the mean seasonal cycle at each grid point and then averaged for the winter season (DJFM). The EOFS were obtained from a singular value decomposition of the covariance matrix of P fields. Finally, the first ten EOFs were orthogonally rotated applying a “Varimax” rotation (Richman, 1986). The aim of the EOFs rotation was to reduce the mode complexity in order to obtain a more physical interpretability of the modes. The percentage of P variance accounted for by the ten selected rotated EOFs was 90.1%. Seven of them (accounting for 72% of the variance) were similar to those found by the NOAA Climate Prediction Center (http://www.cpc.ncep.noaa.gov/data/teledoc/telecontents.shtml) using monthly Z500 fields from NCEP/NCAR atmospheric reanalysis (Kistler et al., 2001) spanning the period 1950-2010. These were the SCAN (19%), NAO (16%), West-Pacific (WP) (10%), EA/WR (9%), Pacific-North American (PNA) (7%), Tropical-Northern Hemisphere (TNH) (6%) and EA (5%). The corresponding PCs of the leading rotated EOFs with a strong signal over the North Atlantic wave climate (Izaguirre et al, 2011; Shimura et al., 2013) were finally selected; they correspond to the indices NAO, EA, EA/WR and SCAN, which were used as independent variables to obtain the parameters of the regression models M12, M13 and M14. A model including the ten PCs was rejected because it did not result in any significant improvement. The same fixed-pattern method described in section 2.2 was used to obtain projections of the climate indices during 1950-2100. That is, simulated winter anomaly fields of P from ECHAM were projected onto the selected rotated PCs derived from the ERA40 reanalysis. The resulting climate indices were finally introduced in models M12 to M14 to obtain SWH anomalies during 1950-2100.

Models M1-M14 simulate total SWH. We further used two additional models: M15, describing the wind sea (SWHw) field, and M16, describing the swell component (SWHs). Winter (DJFM) anomalies of SWHw and SWHs were obtained from HE40 in the same way as for SWH and regressed against atmospheric variables from ERA40. The independent parameters used as predictors were winter anomaly W for SWHw (adequate to describe the local character of the field) and the corresponding PCs of W (accounting for large-scale processes) for SWHs. In order to provide estimates for total SWH, the relationship between this field and its components SWHw and SWHs was used. At quasi-instantaneous (3h) scales SWH, SWHw and SWHs from HE40 verify:

$$SWH^2 = SWHw^2 + SWHs^2 \qquad (1)$$

In order that the same relationship holds at seasonal scales the winter (DJFM) average was applied to the 3-hourly squared fields of SWH. In this way the winter (DJFM) averages $< SWHw^2 >$ and $< SWHs^2 >$ simulated with M15 and M16 can be combined to obtain winter SWH as:

$$< SWH >= \sqrt{(< SWHw^2 > + < SWHs^2 >)} \qquad (2)$$

3. Validation of present-day simulated wave climate

The performance of all (dynamical and statistical) models was first evaluated for the present climate, using HEI as the basis for the evaluation. Altimetry SWH was also used for completeness, but only for some representative models (see Appendix A and Supplementary information, in particular Fig. S2). The validation process is schematically shown in Fig. 2, while the details are given in the sections below.

3.1 Dynamical simulation

The means and variances of winter (DJFM) averaged SWH fields derived from the historical run (DynHist) and the hindcast (HE40) are shown in Figs. 3a-d. The spatial patterns of the means are broadly similar, but DynHist shows higher values (differences of up to 0.5-1m) over most of the domain. The origin of such differences is that the winds in DynHist are stronger (by 0.9 m/s on average) than in HE40 over the North Atlantic (not shown). Differences in SWH of similar magnitude (-0.54 m) were found between HEI and altimetry (Fig. S2). These values are similar to previous works carried out in the North Atlantic, which reported biases ranging from -0.2 to 0.6 m (Ardhuin et al., 2010; Roguers et al., 2012; Reguero et al., 2012). Regarding the variances, both DynHist and HE40 show maximum values of similar magnitude in the north-eastern sector of the domain (Fig. 3c-d). Also the two variance patterns show some differences at regional scale (e.g., in the Bay of Biscay and west of Ireland), although the spatial averaged variance is similar (0.1 m^2).

3.2 Statistical simulations

The stability of the regression parameters of the statistical models was tested by estimating the parameters for the period 1958-1988 (using HE40) and then using the parameters to predict SWH for the HEI period 1989-2009. Models M10, M11, M14 and M17 were also compared with altimetry (for the period 1991-2009) in terms of bias, unbiased root mean square differences (URMSD) and variance accounted for (Fig. S2). The comparison revealed that, in terms of bias, statistical models M17 (-0.42 m) and M10 (-0.46 m) were in slightly better agreement with altimeter data than HEI (-0.54 m), while HEI accounted for the highest percentage of variance.

Figure 4 shows linear trends of statistically simulated winter SWH during the period 1989-2009 fed with ERA-Interim. Coloured areas denote statistical significance (F-test) of the trend at a 5% level. They must be compared with the trends obtained from HEI (Fig. 6a), which show negative values of up to -4 cm/yr over the northern sector of North Atlantic. Such negative trends had already been obtained by other authors; e.g. Young et al. (2011) obtained trends of -2.5 cm/year for the period 1985-2008, although they used annual SWH values from altimeter observations over large regions of the North Atlantic. Most of the models based on statistical downscaling (M1-M11) are able to reproduce the HEI trend pattern; the exceptions are those including P or its PCs as unique predictors: M1, M5 and M8 (Figs. 4a, e, h). The models based on climate indices (M12-M14) show only weak negative trends over the northern sector (Figs. 4l-n).

The percentages of variance of winter SWH from HEI accounted for by each statistical model are mapped in Fig. 5. Models M3, M7 and M10 account for a considerable amount of variance over large areas; on the contrary, M1 shows values lower than 50% everywhere. The spatial averaged fractions of variance captured by the best models are 44% (M3), 51% (M7) and 68% (M10); local values reach up to 97% in some areas, especially at mid and high latitudes.

Figure 6 shows the trends (computed over the validation period 1989-2009) of winter SWH, SWHw and SWHs for the HEI hindcast, the statistical models M15, M16 and the combination of both models according to equation 2. Similarly to M5-M11, a value of n=6 PCs was used to run M16. Hindcasted winter SWH and SWHw trends (Figs. 6a, b) are very similar in magnitude, especially at high latitudes, while the contribution of SWHs to the total trend is much lower, with maximum values of 2 cm/yr over reduced areas at high and mid latitudes, particularly in the Bay of Biscay (Fig. 6c). Statistical models for the two components were able to represent the main features of the observed winter SWH, SWHw and SWHs trends (see Figs. 6d-f). Regarding the accounted variance, M15 was able to recover a high percentage (77% on average) of the hindcasted SWHw, while M16 recovered a small percentage (37% on average) of the hindcasted SWHs. The agreement for the wind component was high over all the domain, reaching 99% of explained variance in some regions (Figs. 6g, h). The agreement for the swell component was higher over the SW sector of the domain, where M16 reached a 93% of explained variance coinciding with swell-dominated areas (sometimes referred to as 'swell pools', see Semedo et al., 2011). However, along a significant part of the European coasts, particularly to the North of the Bay of Biscay, the swell component is poorly recovered by the M16 model. This is a key issue, since swell is the dominant component of the wave climate in those areas (Semedo et al., 2011). Overall, the models M10 and M17 explained the highest percentages of winter SWH variance, with values of 70% (Fig. 5j) and 67% (Fig. 6g).

4. Projections of wave climate for the 21st century

4.1 Dynamical projection

Winter SWH trends for 2000-2100 obtained from the DynProj simulation under the A1B scenario are shown in Fig. 7a. White dots denote statistically non-significant (F-test) trends at the 5% confidence level. The projection shows negative (significant) trends over the North Atlantic, with values of -0.7 cm/yr above 30ºN latitude. Below 30ºN latitude trends are also negative, with values of -0.3 cm/yr. These results are consistent with previous studies based on dynamical approaches. For instance, Hemer et al. (2012) obtained a decrease of up to ~0.7m in annual SWH over the North Atlantic between 1979 and 2099, with higher decreases (~1m) during winter season (they used

ECHAM5 wind fields under a SRES A2 scenario to force the WaveWatch III model; see Tolman, 2009 for details on the model). In the same line, Semedo et al. (2013) showed a decrease of up to 10% (~0.5m) in winter (DJF) SWH between 1959 and 2100 over the North Atlantic (they used high-resolution surface winds from ECHAM5 under A1B scenario to force the WAM model).

The linear winter trends of the two components of SWH (Figs. 7b, c) show different spatial patterns. SWHw shows negative changes in excess of -0.6 cm/yr at mid latitudes and in the NW sector of the North Atlantic, and positive (although non-significant) trends between 20-30ºN, mainly in the eastern sector, in the area under the influence of the Trade winds. SWHs shows smaller (in absolute value) trends than SWHw; they are between -0.1 cm/yr and -0.2 cm/yr over most of the domain, reaching -0.4 cm/yr around 38-40ºN and 45ºW. All these trends (Figs. 7a-c) will be used in the following as the basis for comparison with the statistical models.

In order to give a more complete description of the future wave projections provided by DynProj, the trends of both winter mean wave period (MWP) and mean wave direction (MWD) are also shown in Figs. 7d and 7e. The simulation shows small but statistically significant negative MWP trends over the North Atlantic (-0.4 s/century, on average) reaching maximum values (-0.7 s/century) over the Canary Islands. These results are in agreement with Semedo et al.(2013), who showed an overall decrease in DJF MWP of up to 5% (~0.5s). Significant clockwise trends in MWD of about 10 deg/century are projected at 24ºN-36ºN latitudes reaching maximum values of 35 deg/century over the western sector. Conversely, counter-clockwise trends of about -10deg/century are projected over the north-western sector, reaching maximum values of up to -35 deg/century at 36ºN-48ºN latitudes. This trend pattern is in agreement with those projected by Hemer et al. (2012) and Andrade et al., (2007).

4.2 Statistical projections

Winter SWH trends during 2000-2100 (A1B scenario) obtained using the statistical models M1-M11 are mapped in Fig. 8 (a-k). Averaged values of explained variance and trend differences with DynProj are listed in Table 1. Most of the models show very weak trends over most of the domain. The exceptions are the models including W as a predictor, namely M3, M7 and M10, which show trend patterns and values closer to DynProj (Figs. 8c, g, j). The variance accounted for by each statistical model is shown in Fig. 9. It is worth noting that models were detrended before the calculation of the explained variance, so that the latter does not include the variance associated with the trend. The variance accounted for is highest for M10, with an average value of 68% (Table 1) and a maximum of 95% in the north-central part of the basin, followed by M7 (51% on average and a maximum of 94%), M3 (44% on average and a maximum of 91%) and M11 (33% on average and a maximum of 90%).

Models based on climate indices (M12-M14) yielded very weak winter SWH trends (Figs. 7l-n) and only accounted for a small fraction of the variance (Figs. 9l-n). For example, M14, which includes all four climate indices as independent parameters, accounted for 23% of the variance on average (Table 1), with maximum values of 72% (Fig. 9n). Climate indices accounted for SWH variance regionally. The EA index-based model (M13) accounted for 78% of the variance at 48ºN latitude (Fig. 9m) and the NAO index-based model (CM1) for 71% over the North Sea (Figs. 9l).

The results of the statistical models that address separately winter SWHw and SWHs are mapped in Fig. 10, together with the total winter SWH estimated from the combination of the two components. The M15 and M16 models reproduce the spatial patterns of winter trends obtained from the dynamical model (Figs. 7b-c) but with slightly smaller values in the case of M16 (Figs. 10b-c). Regarding the explained variance, M15 accounts for a large amount of winter SWHw variance (80% on average, with maximum values of up to 98%, Fig. 10e), while M16 accounts for a smaller fraction (34% on average, with large values only in the SE sector of the domain, where it accounts for up to 83% (see Table 1). When both contributions are combined (Figs. 10a,d), the spatial patterns of the trends and the variances accounted for are very similar to those obtained with M3 and M10. The negative trends obtained for SWH (reaching -0.9 cm/yr) are stronger than those obtained with DynProj. In terms of variance, the combined model (M17) accounted for 64 % of the DynProj variance on average (Table 1), reaching values of up to 96% in some areas. These results suggest that the statistical modelling of the wave field benefits from a separate modelling of the wind and swell components.

In addition to the trends and for comparison with the DynProj used as a reference, we also plotted the time series of the simulations DynProj, M3, M7, M10 and M17 at the grid point where the strongest trends were found, namely 50ºN, 50ºW. The results are shown in Figure S3 and display very similar inter-annual variations in all simulations, indicating a good correspondence at these time scales among all models.

5. Discussion and conclusions

The ability of a statistical downscaling method based on 17 different combinations of predictors to project future changes in the wave climate of the North Atlantic Ocean has been explored. Statistical models have been calibrated during the period 1958-2002 by using atmospheric fields from ERA-40 reanalysis and wave fields from a dynamical hindcast (HE40). Another dynamical wave hindcast (HEI) and altimetry observations have been used to validate the statistical models. The changes projected by a dynamical wave model run for the period 2000-2100 are used as reference for the comparison. The reference dynamical projection (an ECHAM5 simulation run under the emission scenario A1B) shows a decrease of SWH over the North Atlantic, especially at high latitudes, which is in agreement with other works (e.g. Hemer et al., 2012, Semedo et al., 2013, Wang et al., 2014).

Previous works like the one by Wang and Swail (2006) had found that wave climate projections are sensitive to the choice of the forcing (in particular the selected GCM), while others like the one by Hemer et al (2013) pointed to the downscaling method (including the regional climate model) and to the choice between dynamical or statistical approach as major uncertainty sources. Our study complements these results by demonstrating three main issues pointed out in the following.

The first one is that among the statistical models used in our study (transfer functions of the seasonally averaged wave fields), the models resulting in better agreement with the dynamical simulation (in terms of winter inter-annual variability and trends) are those using the wind as predictor. Namely, the use of wind speed as independent variable makes that statistical models can account for a significant part of the winter SWH inter-annual variability (68% on average for the model M10) and reproduce the long term changes shown by dynamical projections to a large extent. Regression models that use sea level pressure and/or its gradient on seasonal time scale as independent variables can also account for a part of the inter-annual variability of winter SWH (from 6% to 33% on average), but they cannot reproduce the dynamically projected long term trends over the North Atlantic. It is important to note, however, that wind is a difficult variable to project. The latest Intergovernmental Panel on Climate Change Assessment Report (IPCC AR5, 2013) states that there is a high uncertainty associated with future winds and storms (Bindoff et al., 2013). This is the reason why many statistical models use SLP fields to project SWH, instead of winds (e.g. Wang et al., 2010; Wang et al., 2012; Wang et al., 2014; Casas-Prat et al., 2014). The point to be underlined from our work is that efforts should focus on reducing the uncertainties of projected wind fields, as this reduction would likely translate into more reliable projections of wave climate.

A second issue dealt with in this work is the use of climate indices as predictors. The most important climate pattern over the North Atlantic is the NAO (Rogers et al., 1990) and its influence on wave climate has been discussed for more than a decade (Woolf et al., 2002; Bertin et al., 2013; Feng et al., 2014a,b). Hemer et al. (2013), for instance, forecasted negative SWH changes over almost the entire North Atlantic by the end of the 21st century using a CMIP3 ensemble, while at the same time they forecasted increases in the NAO index. This is consistent with observational studies (for example Woolf et al., 2002) that show a negative correlation between SWH and the NAO index at mid latitudes, but it is contradictory for the northern sector of the North Atlantic, where they are positively correlated. It should be noted, however, that dynamical GCMs run with increasing GHG are not in agreement with each other regarding the future behaviour of the NAO index: while Feng et al. (2014a) did not find a significant NAO trend during the 21^{st} century using the MSLP fields of the CMIP5 ensemble under a RCP85 scenario, Cattiaux et al. (2013) found negative NAO trends using a different method. Even though a negative trend of the NAO index could be related to the negative SWH changes projected by Wang et al. (2014) over the northern sector of the North Atlantic, it could not explain the negative SWH changes projected at middle latitudes. What we have shown is that the NAO index alone is not capable of describing the wave field over the north Atlantic. Even when the four major regional climate indices over the North Atlantic are used, the statistical modelling is not sufficiently good. The same applies to the present climate, when it has been shown that the four climate indices account for only a part of winter SWH variability (Martínez-Asensio et al., in press). The non-stationarity of the relationships between wave parameters and climate indices may also be relevant. In this line, Hemer et al. (2012) found significant changes in the SWH-NAO relationships under warming conditions, especially over the Bay of Biscay.

The third issue demonstrated in this work is that the combination of two regression models, one for wind waves and another one for swell, based on different independent parameters, can improve the projected wave fields. And this is in spite of the limited performance of the statistical models for the swell component over a large part of the domain.

Summarizing, this study highlights the importance of the selection of the independent variables in the statistical models and demonstrates the uncertainty involved in simulating future wave climate on the basis of such statistical models. It must be noted that all regression models were tested using seasonal statistics of wave climate. If higher frequency processes were analyzed (e.g. storm events) the conclusions of the comparison may differ. The conclusions of this study are also relevant for future studies involving the outputs from the new developed CMIP5 models. A way to assess the uncertainties would be to rely only on those statistical methods that use winds as a predictor. The problem in this case is that there is a significant spread in the projections of winds, so the use of a large number of GCMs (i.e. from the new developed CMPI5 or the on-going CMIP6) would be recommended in order to better resolve the uncertainties.

Acknowledgements

This work initiated in the framework of the projects VANIMEDAT-2 (CTM2009-10163-C02-01, funded by the Spanish Ministry of Science and Innovation and the E-Plan of the Spanish Government) and ESCENARIOS (contract funded by the Agencia Estatal de METeorología); in its latter stage its has been partly supported by the project CLIMPACT (CGL2014-54246-C2-1-R, funded by the Spanish Ministry of Economy). A. Martínez-Asensio acknowledges an FPI grant associated with the VANIMEDAT-2 project. M. Marcos and G. Jordà acknowledge a “Ramón y Cajal” contract funded by the Spanish Government. M.N. Tsimplis and X. Feng acknowledge Lloyd's Register Foundation, which supports the advancement of engineering-related education, and funds research and development that enhances safety of life at sea, on land and in the air. The final version of this work has been significantly improved thanks to the suggestions of three anonymous reviewers.

Appendix A

The along-track high-resolution SWH observations used to calibrate the hindcasts were obtained from the Ifremer altimeter Hs database (Queffeulou and Croizé-Fillon, 2010). This database consists of calibrated (Queffeulou, 2004) SWH measurements from seven altimeters (Jason-1, Jason-2, Topex/Poseidon, European Remote Sensing (ERS-1 and ERS-2), Envisat and Geosat Follow-On) spanning the period from January 1991 to December 2009. Along-track SWH observations were first aggregated onto a regular 2x2 degree grid and monthly averaged. Only those grid points with more than a 10% of the maximum number of available observations per cell (N = 96412) were selected. Gridded SWH data were then linearly interpolated onto a 1x1 degree grid. Finally, winter (DJFM) averaged fields were calculated. The comparison between altimeter and modelled winter SWH fields was done in terms of bias, URMSD and percentage of variance accounted for during the period 1991-2009 (see Fig. S2).

Appendix B.

The Stepwise regression method used for statistical models with more than one predictor is illustrated with an example (see Table S1): the fitting of model M7 at a specific grid point (-40ºW, 50ºN). The method first selects the most correlated dependent variable (the one with the less p-value of an F-statistics) and removes its influence through a regression analysis. Then it checks for the p-values of the rest of the dependent parameters. The term with a smallest p-value (lower than a value of 0.05) is then included in the model, assuming that there is sufficient evidence that this term has a non-zero coefficient (i.e. the null hypothesis is rejected). Conversely, if a p-value of any term included in the model is higher than 0.1 it is then excluded from the model. It means that there is sufficient evidence that this term has a zero coefficient. This forward/backward procedure is repeated until the model is not improved in terms of its p-value (note that the p-value reflects the total model performance and not that of the individual terms). Three different models are fitted at each step in the example (see Table S1):

Step 1: $SWH = - 5.7e10^{-4}\ PC1$

Step 2: $SWH = - 6.2e10^{-4}\ PC1 - 8.4e10^{-4}\ PC2$

Step 3: $SWH = - 6.5e10^{-4}\ PC1 - 8.4e10^{-4}\ PC2 + 2.9e10^{-4}\ PC3$

The p-values and explained variances for each of these models are shown in Table S1.

References

Andrade, C., H. O. Pires, R. Taborda, and M. C. Freitas, 2007. Projecting future changes in wave climate and coastal response in Portugal by the end of the 21st century. J Coast Res, 50, 263-257.

Ailliot, P., D. Allard, V. Monbet, and P. Naveau, 2014. Stochastic weather generators: an overview of weather type models.

Ardhuin, F., et al. (2010), Semi-empirical dissipation source functions for wind-wave models: Part I, definition, calibration and validation, J. Phys. Oceanogr., 40,1917–1941.

Bertin, X., E. Prouteau, and C. Letetrel, 2013. A significant increase in wave height in the North Atlantic Ocean over the 20th century. Global Planet. Change, 106, 77–83.

Bindoff, N.L., P.A. Stott, K.M. AchutaRao, M.R. Allen, N. Gillett, D. Gutzler, K. Hansingo, G. Hegerl, Y. Hu, S. Jain, I.I. Mokhov, J. Overland, J. Perlwitz, R. Sebbari and X. Zhang, 2013. Detection and Attribution of Climate Change: from Global to Regional. In: Climate Change 2013: The Physical Science Basis. Contribution of Working Group I to the Fifth Assessment Report of the Intergovernmental Panel on Climate Change [Stocker, T.F., D. Qin, G.-K. Plattner, M. Tignor, S.K. Allen, J. Boschung, A. Nauels, Y. Xia, V. Bex and P.M. Midgley (eds.)]. Cambridge University Press, Cambridge, United Kingdom and New York, NY, USA.Casas-Prat M., X. L. Wang, and J. P. Sierra, 2014. A physical-based statistical method for modeling ocean wave heights. Ocean Model, 73:59–75

Camus, P., M. Menéndez, F. J. Méndez, C. Izaguirre, A. Espejo, V. Cánovas, J. Pérez, A. Rueda, I. J. Losada, and R. Medina, 2014. A weather-type statistical downscaling framework for ocean wave climate, J. Geophys. Res. Oceans, 119, 7389–7405.

Cattiaux, J., H. Douville, and Peings, Y.,2013. European temperatures in CMIP5: origins of present-day biases and future uncertainties. Climate dynamics, 41(11-12), 2889-2907.

Charles, E., D. Idier, P. Delecluse, M. Déqué, and G. Le Cozannet, 2012. Climate change impact on waves in the Bay of Biscay, France. Ocean Dynamics, 62(6), 831-848.

Draper, N.R., and H. Smith, 1998. Applied Regression Analysis. Wiley-Interscience, Hoboken, NJ pp. 307–312.

Fan, Y., I., I. M. Held, S.-J. Lin, and X. Wang, 2013. Ocean warming effect on surface gravity wave climate change for the end of the twenty-first century. J. Climate, 26, 6046–6066.

Fan, Y., S. J. Lin, S. M. Griffies, and M. A. Hemer, 2014. Simulated global swell and wind-sea climate and their responses to anthropogenic climate change at the end of the twenty-first century. Journal of Climate, 27(10), 3516-3536.

Feng, X., M.N. Tsimplis, M.J. Yelland, and G.D. Quartly, 2014a. Changes in significant and maximum wave heights in the Norwegian Sea. Global and Planetary Change, 113, 68-76.

Feng, X., M.N. Tsimplis, G.D. Quartly, and M.J. Yelland, 2014b. Wave height analysis from 10 years of observations in the Norwegian Sea. Continental Shelf Research, 72, 47-56.Günther, H., S. Hasselman, and P. A. E. Jansen, 1992. The WAM model cycle, 4. Technical Report 4. DKRZ.

Günther, H., Hasselman, S., & Jansen, P. A. E. (1992). The WAM model cycle, 4. Technical Report 4. DKRZ.

Hasselmann, S., C. Brüning, K. Hasselmann, and P. Heimbach, 1996. An improved algorithm for retrieval of ocean wave spectra from synthetic aperture radar image spectra. J. Geophys. Res., 101, 16 615-16 629

Hemer, M. A., J. Katzfey, and C. Trenham, 2012. Global dynamical projections of surface ocean wave climate for a future high greenhouse gas emission scenario. Ocean Modelling, 70, 221–245

Hemer, M. A., Y. Fan, N. Mori, A. Semedo, and X. L. Wang, 2013. Projected changes wave climate from a multi-model ensemble. Nature Clim. Change, 3, 471–476.

Izaguirre, C., F. J. Méndez, M. Menéndez, and I. J. Losada, 2011., Global extreme wave height variability based on satellite data, Geophys. Res. Lett., 38, L10607, doi:10.1029/2011GL047302.

Kistler, R., E. Kalnay, W. Collins, S. Saha, G. White, J. Wollen, M. Chelliah, W. Ebisuzaki, M. Kanamitsu, V. Kousky, H. van den Dool, R. Jenne, and M. Fioriono, 2001. The NCEP/ NCAR 50-year reanalysis: monthly means CD-ROM and documentation. Bull. Am. Meteorol. Soc. 82, 247–267.

Lorenz, E. N., 1969. Atmospheric predictability as revealed by naturally occurring analogues. Journal of the Atmospheric sciences, 26(4), 636-646.

Martinez-Asensio, A., M.N. Tsimplis, M. Marcos, X. Feng, D. Gomis, G. Jorda, and S. Josey, Response of the North Atlantic wave climate to atmospheric modes of variability, International Journal of Climatology, doi:10.1002/joc.4415, in press.

Mori, N., T. Yasuda, H. Mase, T. Tom, and Y. Oku, 2010. Projection of extreme wave climate change under global warming. Hydrol. Res. Lett., 4, 15–19.

Pérez, J., M. Menéndez, F.J. Méndez, and I. J. Losada, 2014. Evaluating the performance of CMIP3 and CMIP5 global climate models over the north-east Atlantic region. Climate Dynamics, 43(9-10), 2663-2680.

Queffeulou P., 2004. Long term validation of wave height measurements from altimeters, Marine Geodesy, 27, 495-510.

Queffeulou, P., and D. Croizé-Fillon, 2010. Global altimeter SWH data set, version 7, <ftp://ftp.ifremer.fr/ifremer/cersat/products/swath/altimeters/waves/>.

Reguero, B.G., M. Menéndez, F.J. Méndez, R. Mínguez, I.J. Losada, 2012. A global ocean wave (GOW) calibrated reanalysis from 1948 onwards. Coastal Engineering, 65, 38–55.

Richman, M. B. 1986. Rotation of principal components. J. Climatol. 6, 293_335.

Roeckner, E., G. Bauml, L. Bonaventura, R. Brokopf, M. Esch, M. Giorgetta, S. Hagemann, I. Kirchner, L. Kornblueh, E. Manzini, A. Rhodin, U. Schlese, U. Schulzweida, and A. Tompkins, 2003. The atmospheric general circulation model ECHAM 5. Part I: model description.Technical Report 349, Max Planck Institute for Meteorology Rogers, J.C., 1990. Patterns of low frequency monthly sea level pressure variability (1899-1986) and associated wave cyclone frequencies. J. Climate, 3, 1364-1379.

Rogers, J.C.,1990. Patterns of low frequency monthly sea level pressure variability (1899-1986) and associated wave cyclone frequencies. J. Climate, 3, 1364-1379.

Rogers, W.E.; Dykes, J.D.; Wang, D.; Carroll, S.N.; Watson, K. (2012) - Validation Test Report for WAVEWATCH III. 67p, DTIC Document, Slidell, LA, United States of America.

Semedo, A., K. Sušelj, A. Rutgersson, and A. Sterl, 2011. A global view on the wind sea and swell climate and variability from ERA-40. Journal of Climate,24(5), 1461-1479.

Semedo, A., Ralf Weisse, Arno Behrens, Andreas Sterl, Lennart Bengtsson, and Heinz Günther, 2013. Projection of Global Wave Climate Change toward the End of the Twenty-First Century. J. Climate, 26, 8269–8288.

Shimura T., N. Mori and H. Mase, 2013. Ocean waves and teleconnection patterns in the Northern Hemisphere, Journal of Climate, 26, pp.8654-8670

Tolman, H. L., 2009. User manual and system documentation of WAVEWATCH III TM version 3.14. Technical note, MMAB Contribution, 276.

Wallace, J. M., C. Smith, and C. S. Bretherton, 1992. Singular value decomposition of wintertime sea surface temperature and 500-mb height anomalies. Journal of climate, 5(6), 561-576.

WAMDI Group, 1998. The WAM model-A third generation ocean wave prediction model, J. Phys. Oceanogr., 18, 1775–1810.

Wang X.L.L., F.W. Zwiers and V.R. Swail, 2004. North Atlantic ocean wave climate change scenarios for the twenty-first century. J Clim 17:2368–2383

Wang, X. L., and V. R. Swail, 2006. Climate change signal and uncertainty in projections of ocean wave heights. Clim. Dyn., 26, 109–126.

Wang, X. L., V. R. Swail, F. W. Zwiers, X. Zhang, and Y. Feng, 2008. Detection of external influence on trends of atmospheric storminess and ocean wave heights, Clim. Dyn., 32, 189–203.

Wang, X. L., V. R. Swail, and A. Cox, 2010. Dynamical versus statistical downscaling methods for ocean wave heights, Int. J. Climatol., 30, 317–332.

Wang, X. L., Y. Feng, and V. R. Swail, 2012 North Atlantic wave height trends as reconstructed from the twentieth century reanalysis, Geophys. Res. Lett., 39, L18705.

Wang X. L, Y. Feng, and V. R. Swail, 2014. Changes in global ocean wave heights as projected using multimodel CMIP5 simulations. Geophys Res Lett 41(3):1026–1034

Wang, X.L., Y. Feng, and V. R. Swail, 2015: Climate change signal and uncertainty in the CMIP5-based projections of global ocean surface wave heights. JGR-Oceans, 120.

Wilby, R. L., S. P. Charles, E. Zorita, B. Timbal, P. Whetton, and L. O. Mearns, 2004. Guidelines for use of climate scenarios developed from statistical downscaling methods. Supporting material of the Intergovernmental Panel on Climate Change. Task Group on Data and Scenario Support for Impacts and Climate Analysis, Rotherham

Wilks, D. S., 1998. Multisite generalization of a daily stochastic precipitation generation model. Journal of Hydrology, 210(1), 178-191.

Woolf, D.K., P.D. Cotton, and P.G. Challenor, 2002. Variability and predictability of the North Atlantic wave climate. Journal of Geophysical Research 107 (C10), 9–23.

Young, I. R., S. Zieger, and A. V. Babanin, 2011. Global trends in wind speed and wave height. Science, 332(6028), 451-455.

Zorita, E., and H. Von Storch, 1999. The analog method as a simple statistical downscaling technique: comparison with more complicated methods. Journal of climate, 12(8), 2474-2489.

Table and Figure Captions

Table 1. Spatially averaged percentages of variance of DynProj winter SWH (2000-2100, A1B scenario) accounted for by the statistical simulations (M1-M17). Spatially averaged winter SWH trends and the corresponding standard deviation (cm/year). Differences between averaged winter SWH trends of statistical simulations and DynProj (cm/year).

Figure 1. Dynamical and statistical simulations flowchart.

Figure 2. Validation process flowchart.

Figure 3. Mean value and variance of winter (DJFM) SWH fields for DynHist (a, c) and HE40 (b, d) for the common period 1958-1999. Spatially averaged values are also shown.

Figure 4. Winter SWH trends (cm/yr) inferred from the statistical models (a-n) for the period 1989-2009. Coloured areas denote model statistical significance (F-test) at 5% level. Spatially averaged values are also shown.

Figure 5. Percentage of variance of hindcasted winter SWH accounted for by each of the statistical models (a-n) for the period 1989-2009. Coloured areas denote model statistical significance (F-test) at 5% level. Spatially averaged values are also shown.

Figure 6. Linear trends (cm/yr) of winter SWH, SWHw and SWHs for HEI (a-c), M17 (d), M15 (e) and M16 (f) obtained for the period 1989-2009. The percentage of HEI winter SWH, SWHw and SWHs variance accounted for M17, M15 and M16 respectively (g-i). Coloured areas denote model statistical significance (F-test) at 5% level. Spatially averaged values are also shown.

Figure 7. Linear trends of winter SWH (a), SWHw (b), SWHs (c) MWP (e) and MWD (f) obtained from DynProj for the period 2000-2100. White dots denote no statistical significance (F-test) at 5% level. Spatially averaged values are also shown.

Figure 8. Linear trends (cm/yr) of winter SWH obtained from the statistical models (a-n) for the period 2000-2100. Coloured areas denote model statistical significance (F-test) at 5% level. White dots denote no statistical significance (F-test) of the trend at 5% level. Spatially averaged values are also shown.

Figure 9. Percentage of variance of the DynProj winter SWH accounted for each of the statistical models (a-n) for the period 2000-2100. Coloured areas denote model statistical significance (F-test) at 5% level. Spatially averaged values are also shown.

Figure 10. Linear trends (cm/yr) of winter SWH, SWHw and SWHs for M17 (a), M15 (b) and M16 (c) for the period 2000-2100. Percentage of variance of DynProj winter SWH, SWHw and SWHs accounted for M17 (d), M15 (e) and M16 (f). Spatially averaged values are also shown.

Table S1. P-value of each independent variable of the model M7 throughout the stepwise regression procedure at grid point (-40ºW, 50ºN). The percentage of HEI winter SWH variance accounted for M7 at each step is also shown.

Figure S1. Domain of the WAM model in the North Atlantic. Grid points with the different resolutions used in different regions (black dots).

Figure S2. Bias (in meters) (a-e), URMSD (in meters) (f-j) and variance accounted for (in %) (k-o) between winter altimeter SWH and HEI (a, f, k), M17 (b, g, l), M10 (c, h, m), M11 (d, i, n) and M14 (e, j, o) for the period 1991-2009. Coloured areas denote that the statistical regression of the model is significant (F-test) at a 5% level. Spatially averaged values are also shown.

Figure S3. Winter SWH anomaly time series at 50N latitude and -50W longitude projected by DynProj (blue line), M3 (green line), M7 (red line), M10 light blue line) and M17 (purple line).

Table 1. Spatially averaged percentages of variance of DynProj winter SWH (2000-2100, A1B scenario) accounted for by the statistical simulations (M1-M17). Spatially averaged winter SWH trends and the corresponding standard deviation (cm/year). Differences between averaged winter SWH trends of statistical simulations and DynProj (with an averaged value of-0.29cm/year).

Model	Variance account (%)	Mean trend (cm/year)	Std trend (cm/year)	Trend diff. (cm/year)
M1	5.9	-0.04	0.04	0.25
M2	15.1	-0.06	0.10	0.23
M3	43.7	-0.11	0.16	0.18
M4	19.5	-0.07	0.09	0.22
M5	27.4	-0.03	0.04	0.26
M6	22.0	-0.07	0.09	0.22
M7	51.4	-0.17	0.11	0.12
M8	28.1	-0.03	0.05	0.26
M9	27.7	-0.09	0.11	0.20
M10	67.7	-0.19	0.14	0.10
M11	33.1	-0.08	0.10	0.21
M12	2.8	0.01	0.05	0.30
M13	8.7	-0.01	0.01	0.28
M14	23.2	-0.02	0.05	0.27
M15	80.3	-0.12	0.19	0.01
M16	33.8	-0.09	0.05	0.09
M17	63.8	-0.20	0.19	0.09

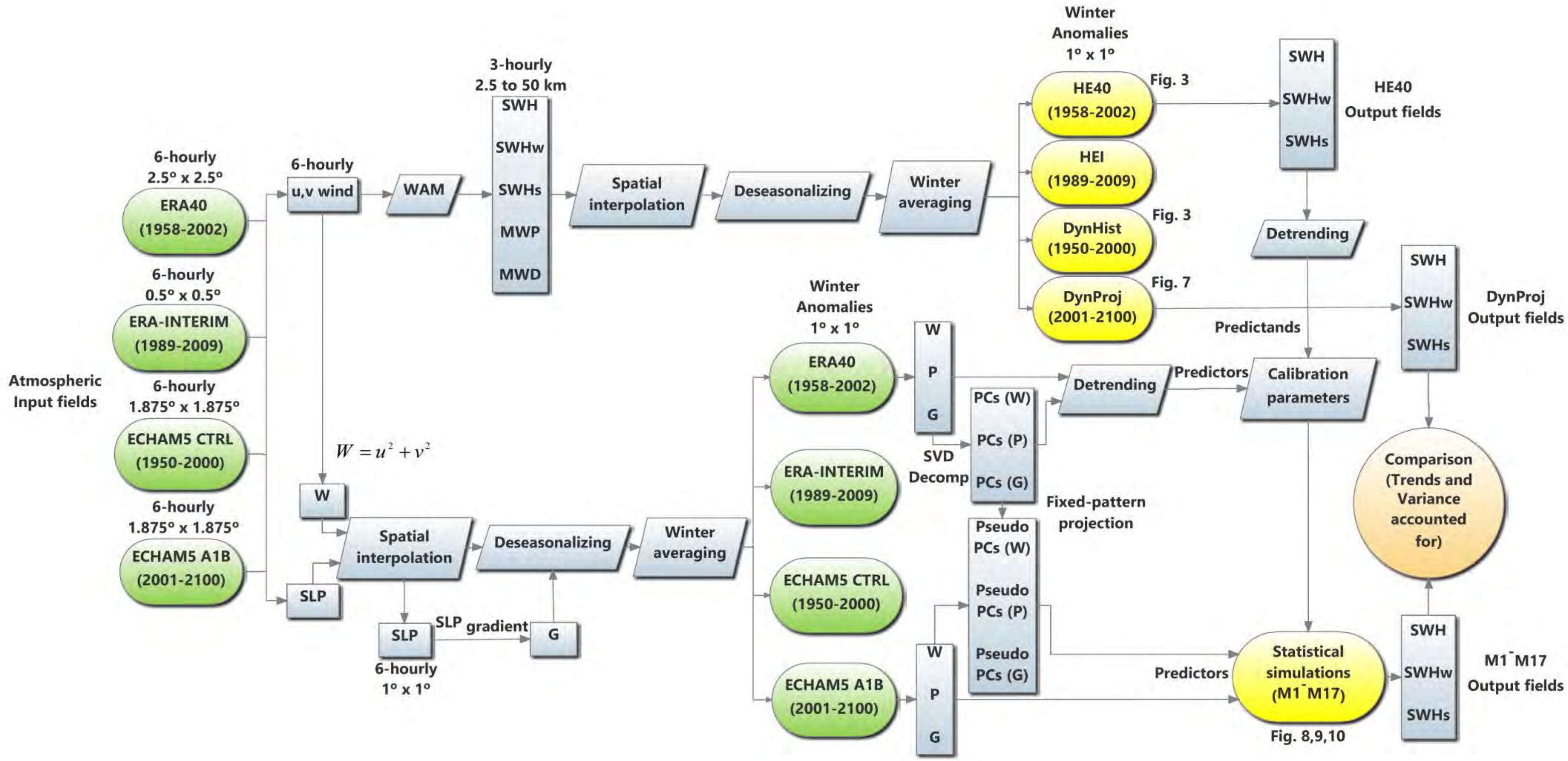

Figure 1. Dynamical and statistical simulations flowchart.

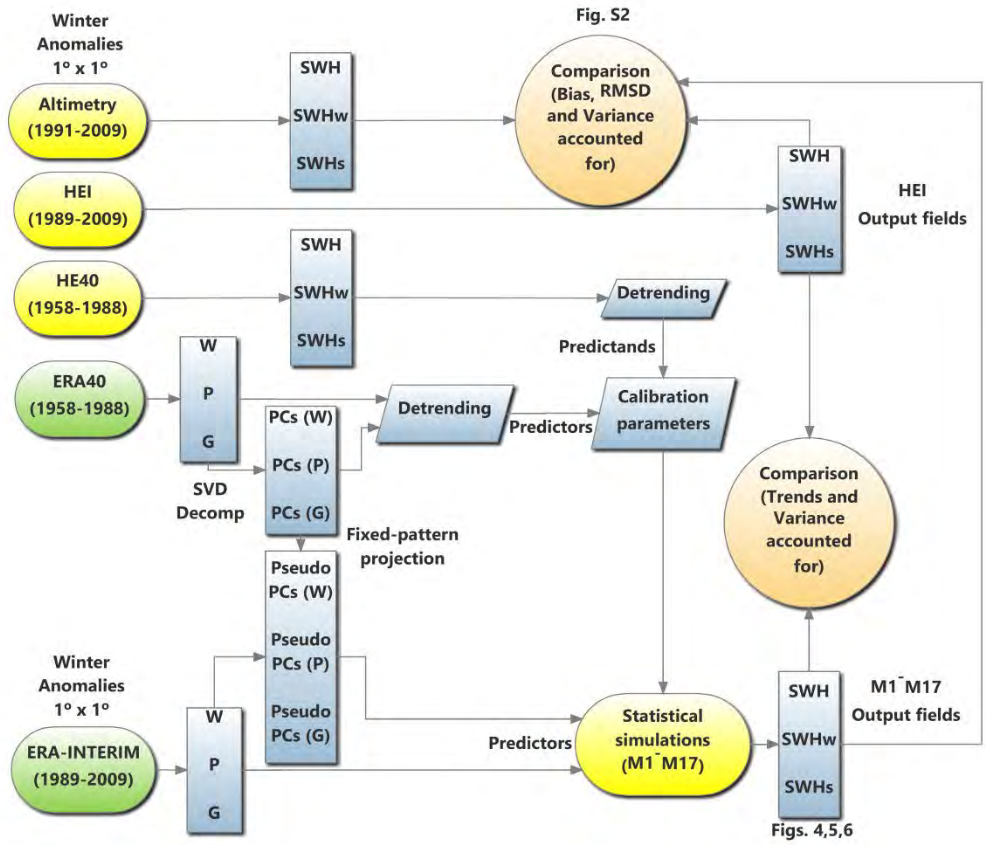

Figure 2. Validation process flowchart.

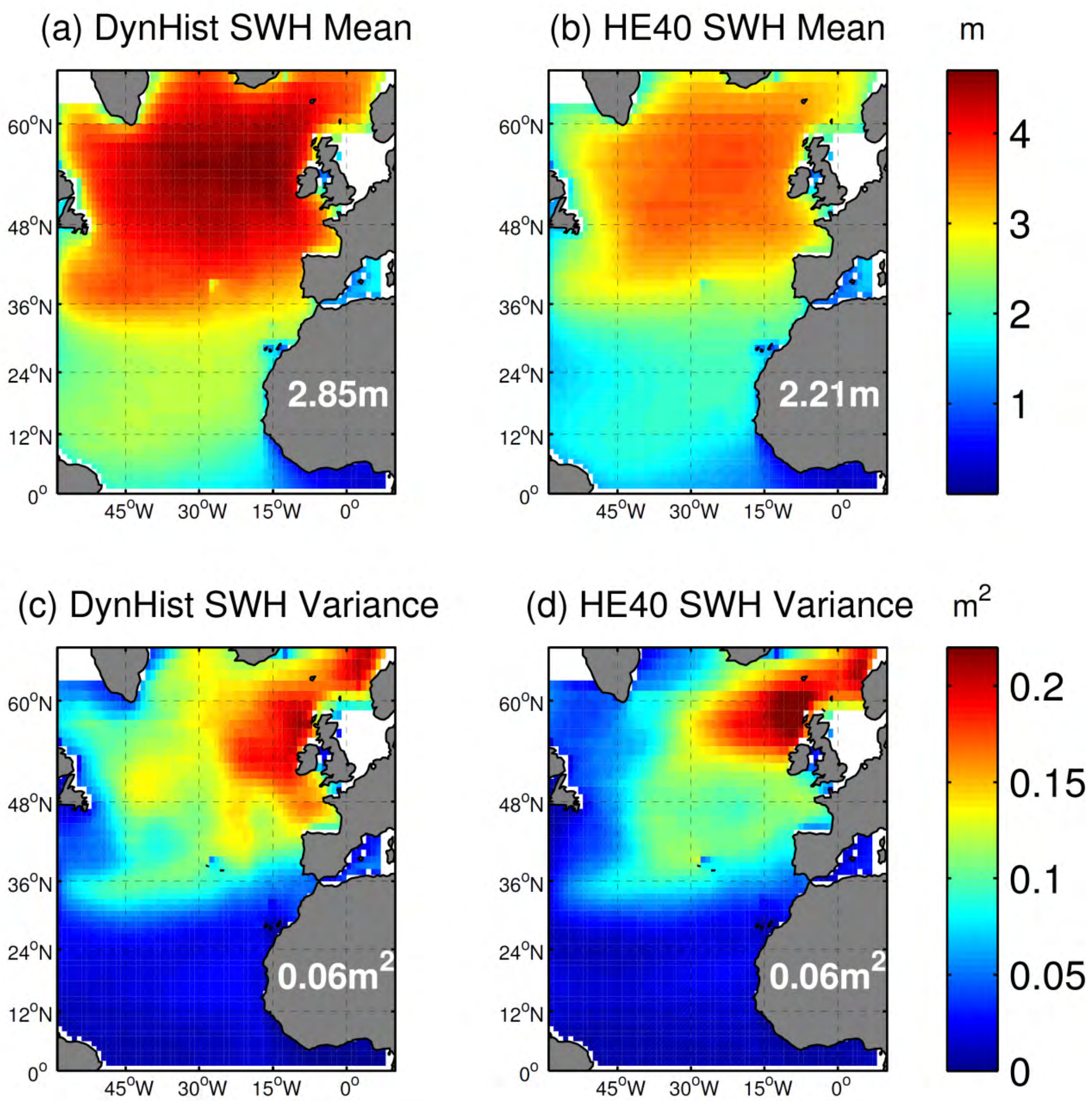

Figure 3. Mean value and variance of winter (DJFM) SWH fields for DynHist (a, c) and HE40 (b, d) for the common period 1958-1999. Spatially averaged values are also shown.

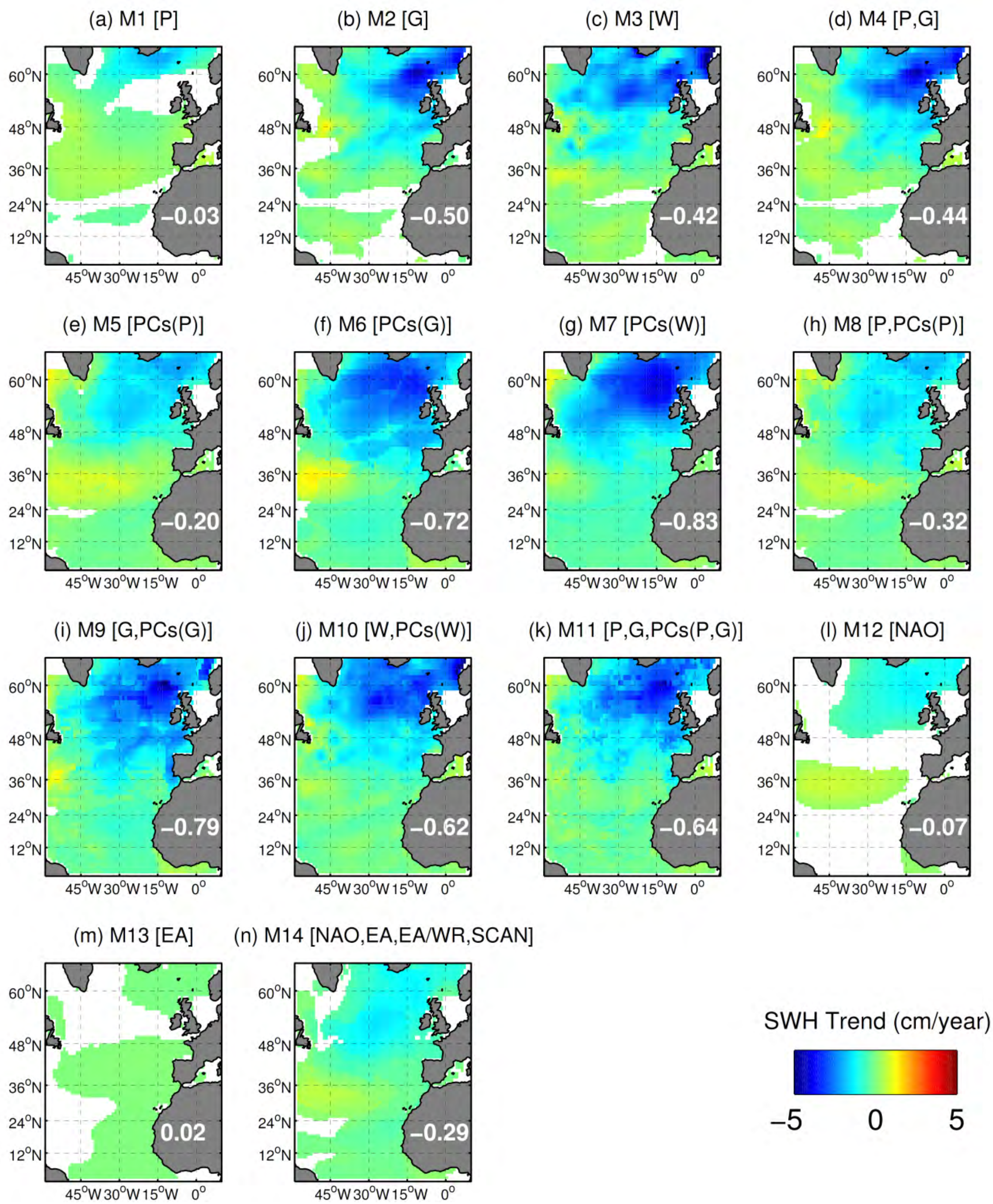

Figure 4. Winter SWH trends (cm/yr) inferred from the statistical models (a-n) for the period 1989-2009. Coloured areas denote model statistical significance (F-test) at 5% level. Spatially averaged values are also shown.

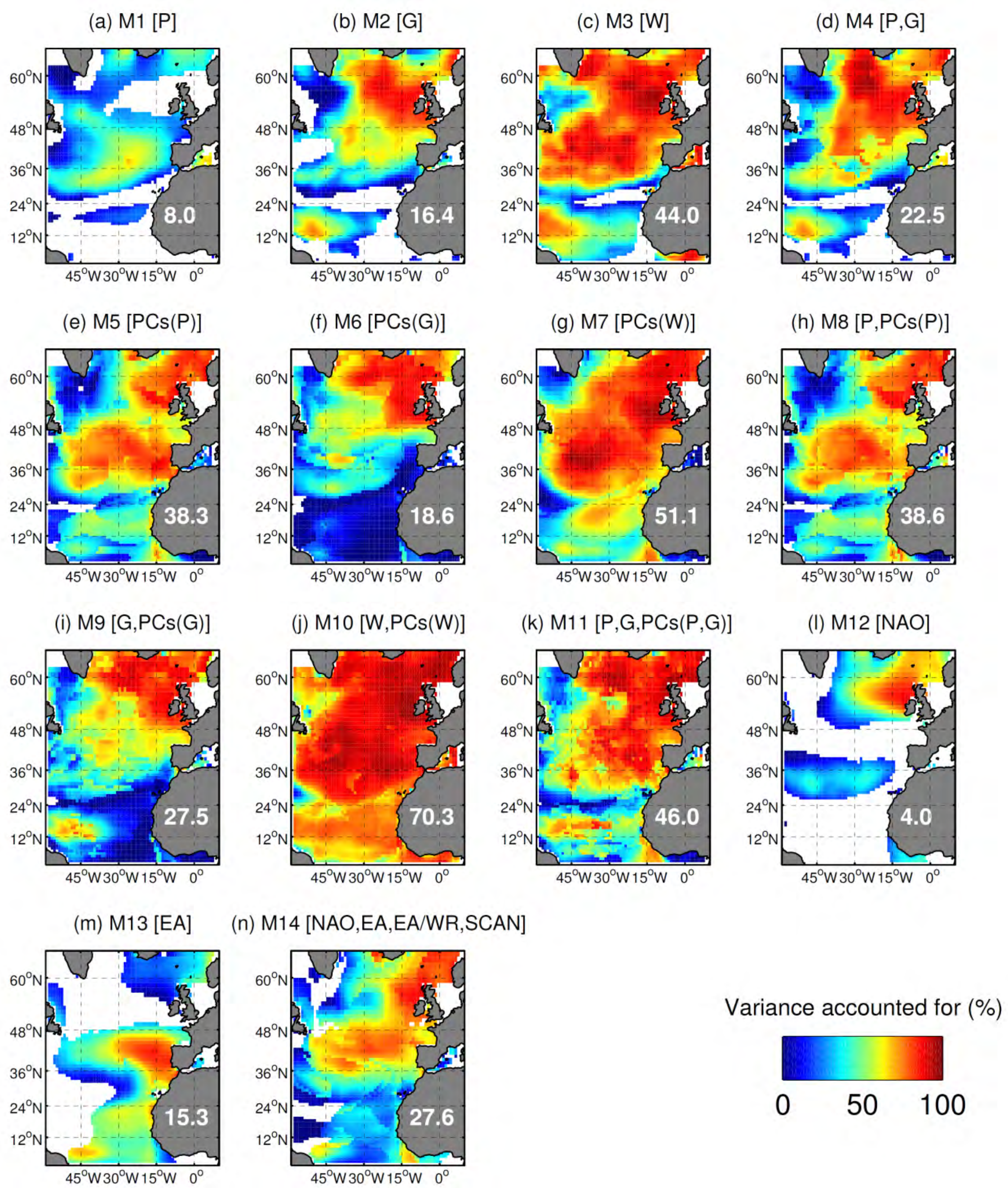

Figure 5. Percentage of variance of hindcasted winter SWH accounted for by each of the statistical models (a-n) for the period 1989-2009. Coloured areas denote model statistical significance (F-test) at 5% level. Spatially averaged values are also shown.

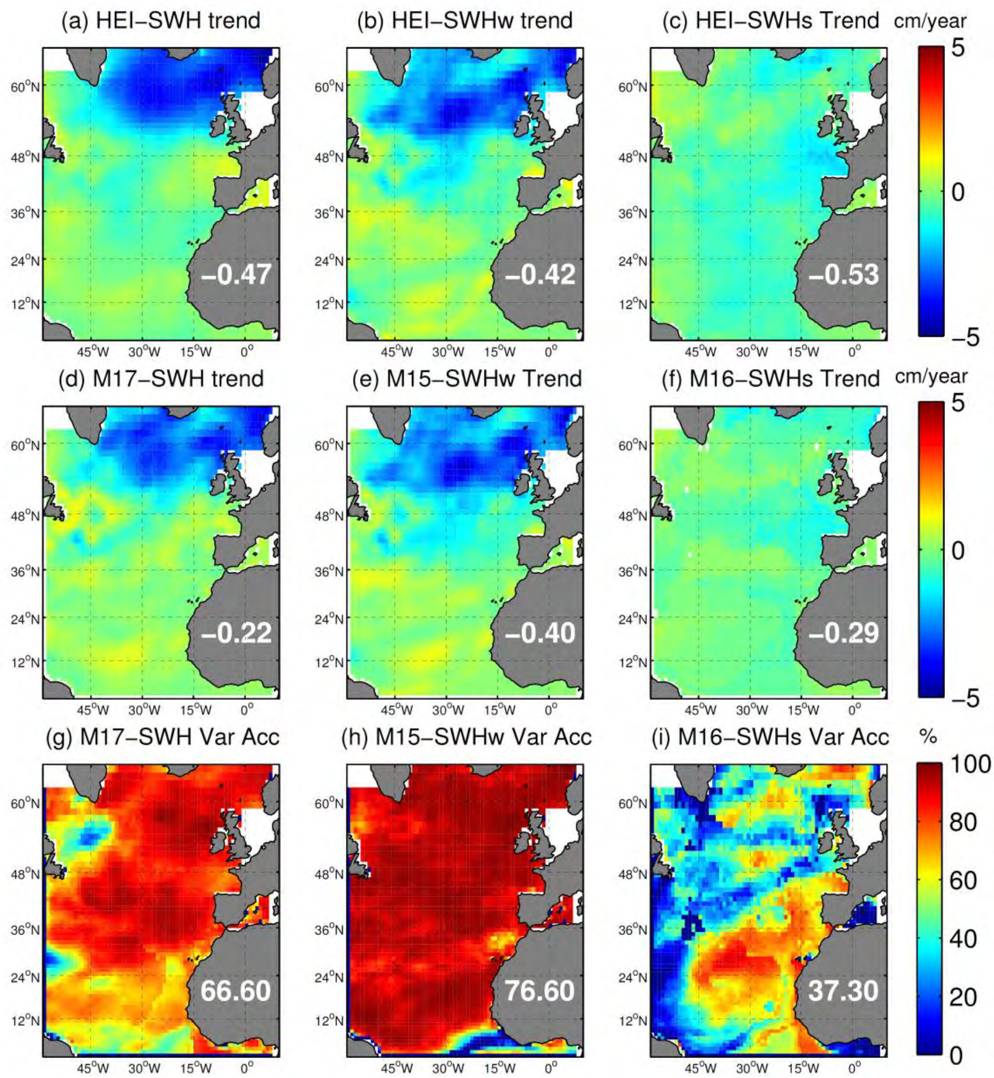

Figure 6. Linear trends (cm/yr) of winter SWH, SWHw and SWHs for HEI (a-c), M17 (d), M15 (e) and M16 (f) obtained for the period 1989-2009. The percentage of HEI winter SWH, SWHw and SWHs variance accounted for M17, M15 and M16 respectively (g-i). Coloured areas denote model statistical significance (F-test) at 5% level. Spatially averaged values are also shown.

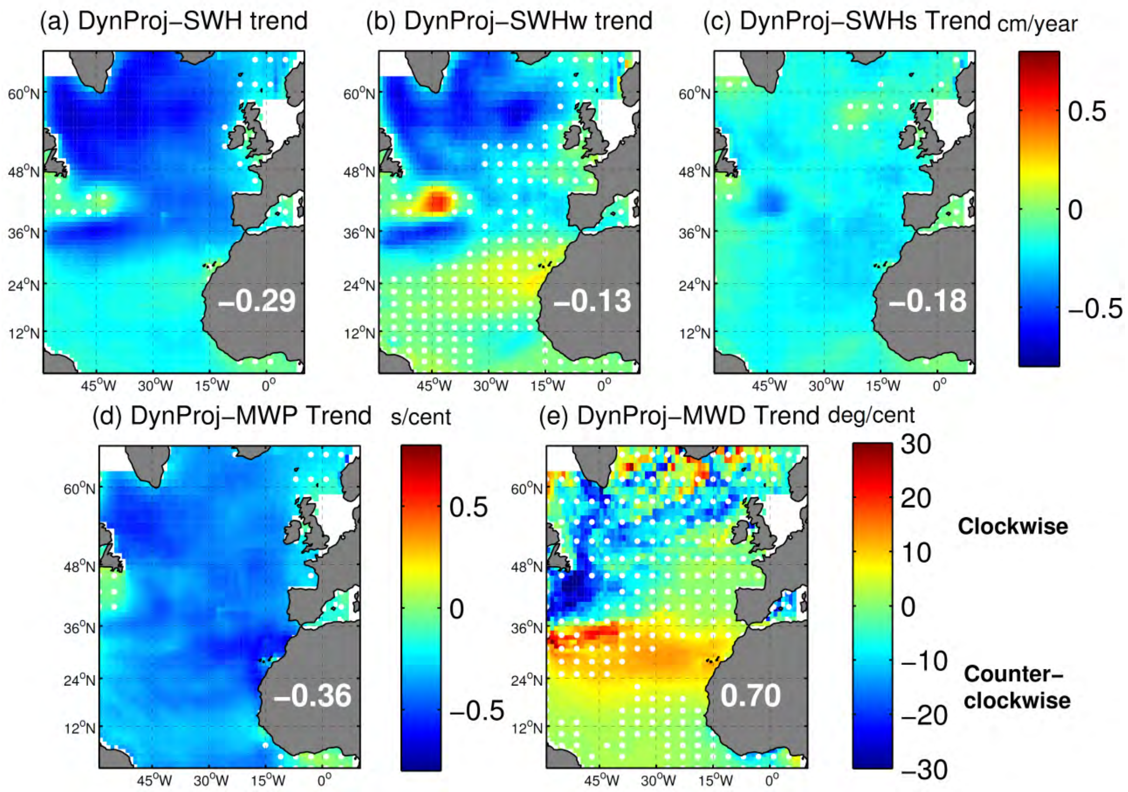

Figure 7. Linear trends of winter SWH (a), SWHw (b), SWHs (c) MWP (e) and MWD (f) obtained from DynProj for the period 2000-2100. White dots denote no statistical significance (F-test) at 5% level. Spatially averaged values are also shown.

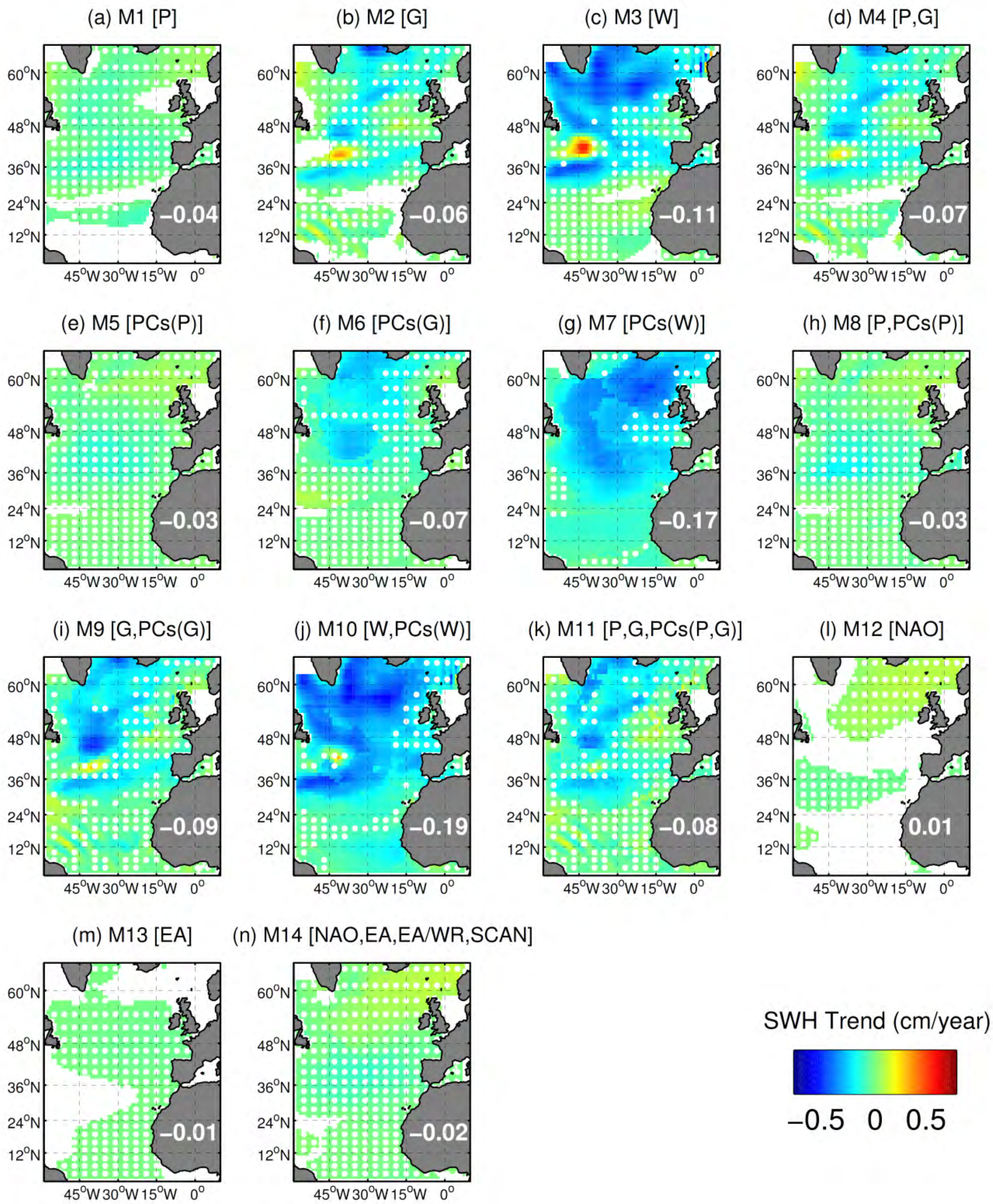

Figure 8. Linear trends (cm/yr) of winter SWH obtained from the statistical models (a-n) for the period 2000-2100. Coloured areas denote model statistical significance (F-test) at 5% level. White dots denote no statistical significance (F-test) of the trend at 5% level. Spatially averaged values are also shown.

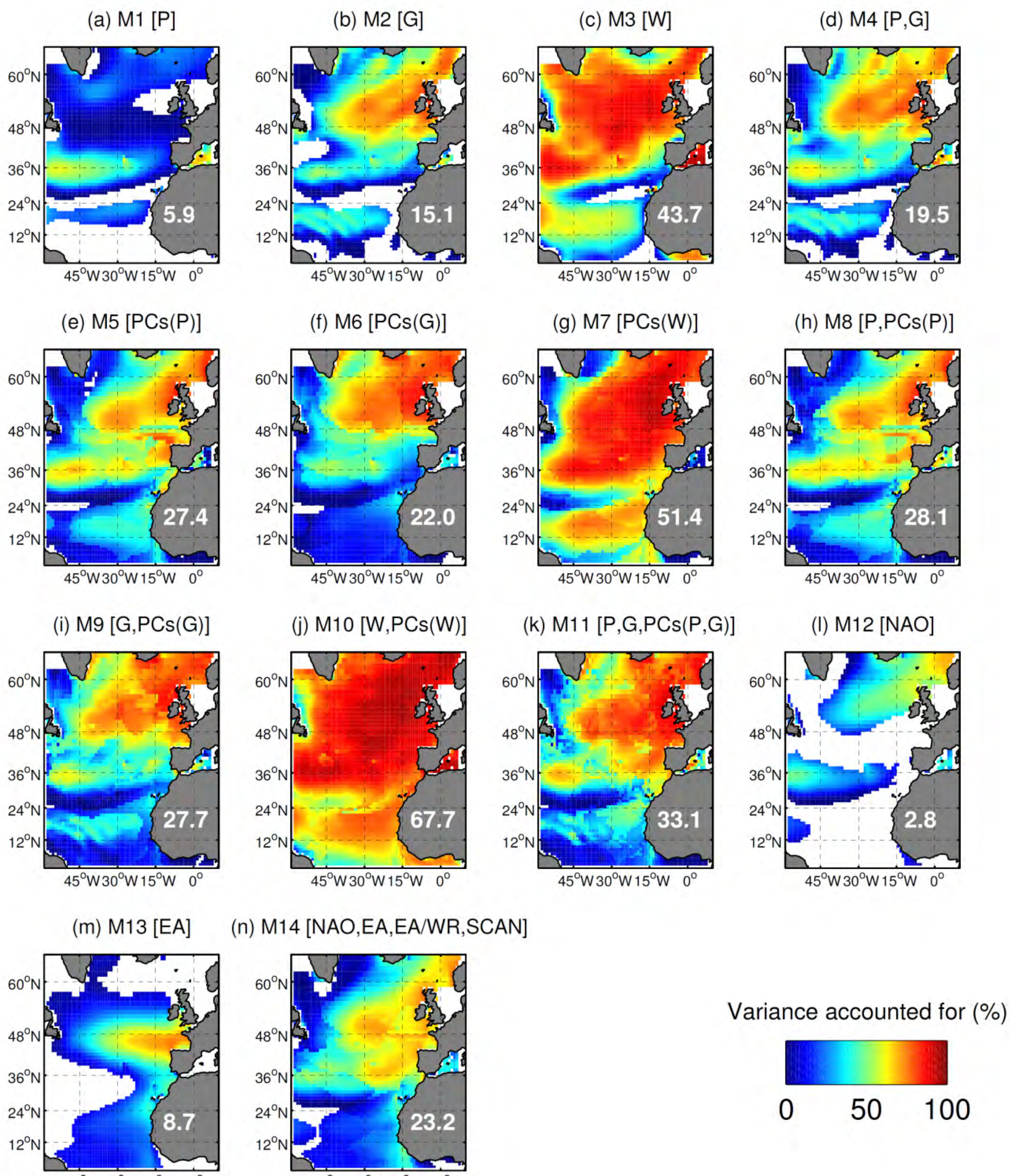

Figure 9. Percentage of variance of the DynProj winter SWH accounted for each of the statistical models (a-n) for the period 2000-2100. Coloured areas denote model statistical significance (F-test) at 5% level. Spatially averaged values are also shown.

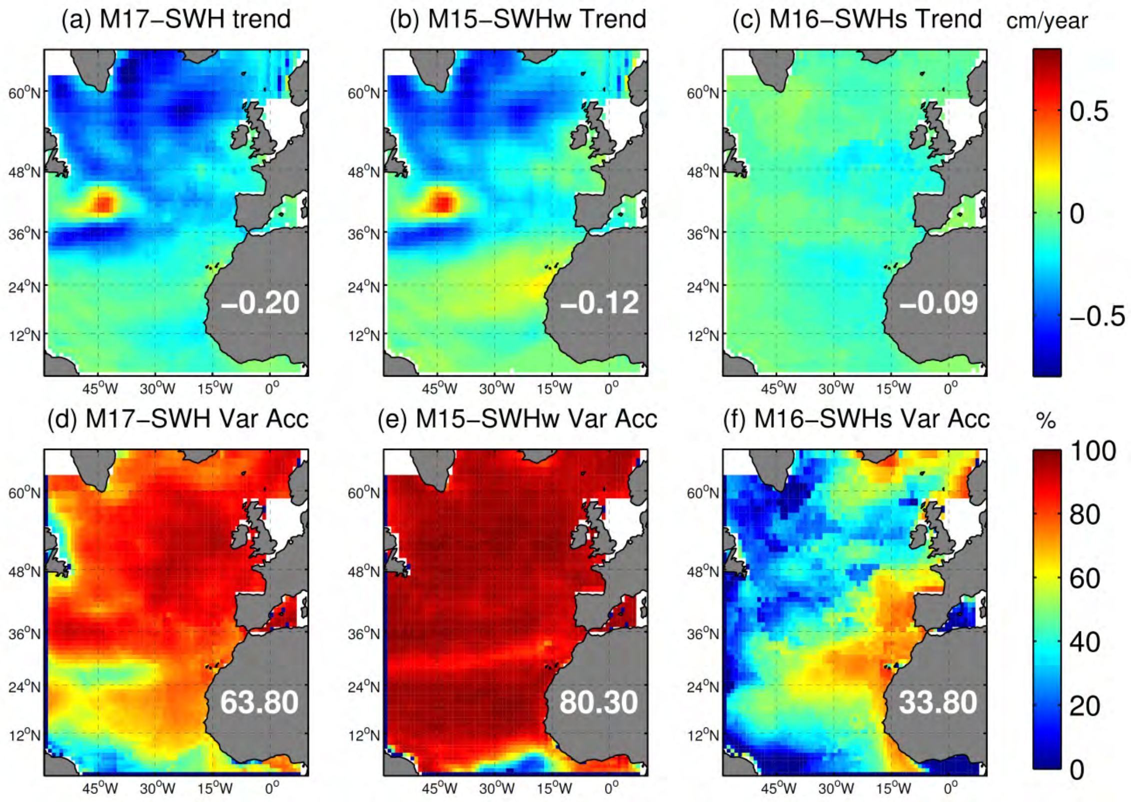

Figure 10. Linear trends (cm/yr) of winter SWH, SWHw and SWHs for M17 (a), M15 (b) and M16 (c) for the period 2000-2100. Percentage of variance of DynProj winter SWH, SWHw and SWHs accounted for M17 (d), M15 (e) and M16 (f). Spatially averaged values are also shown.

__Table S1.__ P-value of each independent variable of the model M7 throughout the stepwise regression procedure at grid point (-40ºW, 50ºN). The percentage of HEI winter SWH variance accounted for M7 at each step is also shown.

	Before stepwise regression		**Step 1: PC1 included**	**Step 2: PC2 included**	**Step 3: PC3 included**
	Corr. Coef.	**Pvalue of an F-statistic**			
PC1	-0.63	0.000007	0.000007	0.000000	0.000000
PC2	-0.54	0.000213	0.000000	0.000000	0.000000
PC3	0.12	0.437032	0.216563	0.032044	0.032044
PC4	0.10	0.507104	0.573319	0.092025	0.063947
PC5	0.30	0.048526	0.531827	0.951542	0.841806
PC6	0.00	0.998939	0.708841	0.425440	0.388856
Var.acc. (%)			40.9	79.5	82.2

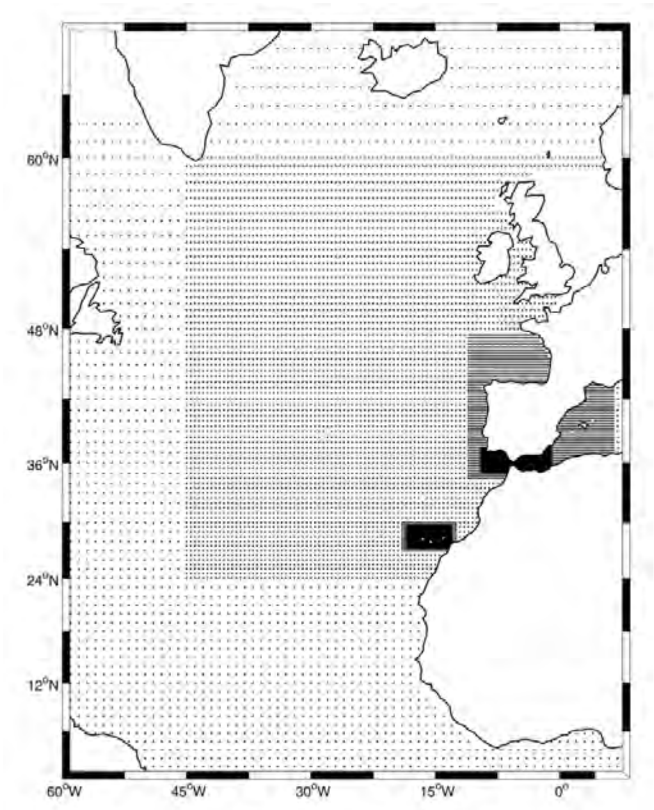

Figure S1. Domain of the WAM model in the North Atlantic. Grid points with the different resolutions used in different regions (black dots).

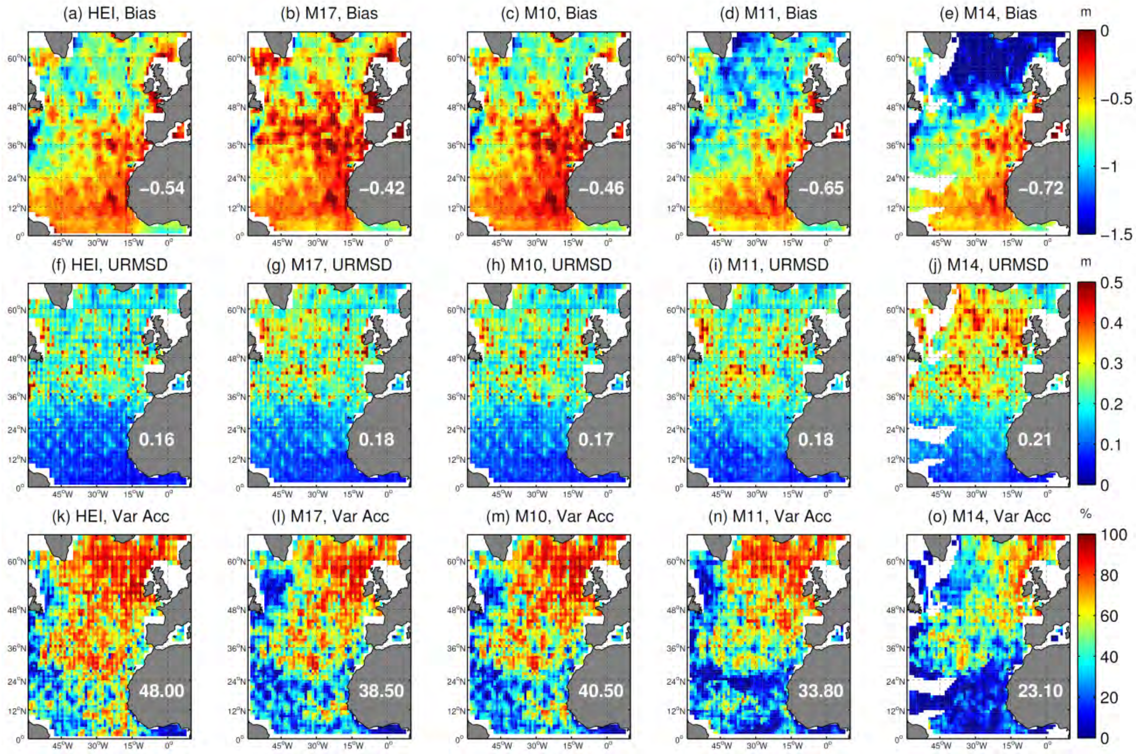

Figure S2. Bias (in meters) (a-e), URMSD (in meters) (f-j) and variance accounted for (in %) (k-o) between winter altimeter SWH and HEI (a, f, k), M17 (b, g, l), M10 (c, h, m), M11 (d, i, n) and M14 (e, j, o) for the period 1991-2009. Spatially averaged values are also shown.

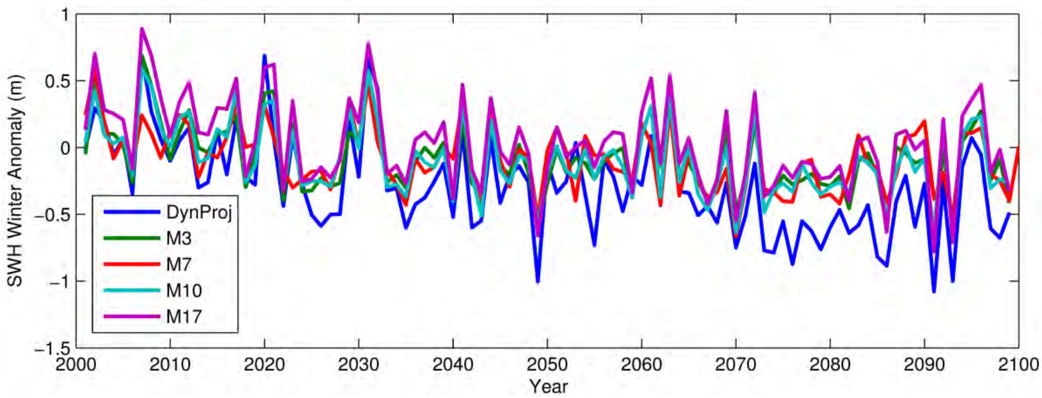

Figure S3. Winter SWH anomaly time series at 50N latitude and -50W longitude projected by DynProj (blue line), M3 (green line), M7 (red line), M10 light blue line) and M17 (purple line).